Thermal Decomposition of Erythritol Tetranitrate: A Joint Experimental and Computational Study

Jimmie C. Oxley[*,1], David Furman[2,3], Austin C. Brown[1], Faina Dubnikova[2], James L. Smith[1], Ronnie Kosloff[2] and Yehuda Zeiri[3,4]

[1]Chemistry Department, University of Rhode Island, Kingston, Rhode Island 02881, United States
[2]Fritz Haber Research Center for Molecular Dynamics, Institute of Chemistry, Hebrew University of Jerusalem, Jerusalem 91904, Israel
[3]Division of Chemistry, NRCN, P.O. Box 9001, Beer-Sheva 84190, Israel
[4]Department of Biomedical Engineering, Ben-Gurion University, Beer-Sheva 94105, Israel

joxley@chm.uri.edu

Abstract

Pentaerythritol tetranitrate finds many uses in the energetic materials community. Due to the recent availability of erythritol, erythritol tetranitrate (ETN) can now be readily synthesized. Accordingly, its complete characterization, especially its stability, is of great interest. This work examines the thermal decomposition of ETN, both through experimental and computational methods. In addition to kinetic parameters, decomposition products were examined to elucidate its decomposition pathway. It is found that ETN begins its decomposition sequence by a unimolecular homolytic cleavage of the internal and external O-NO_2 bonds, while the competing HONO elimination reaction is largely suppressed. The global activation energy for decomposition is found to be 104.3 kJ/mol with a pre-exponential factor of $3.72 \cdot 10^9$ s^{-1}. Despite the ability to exist in a molten state, ETN has a lower thermal stability than its counterpart PETN.

Introduction

Although erythritol tetranitrate (ETN), an explosive nitrate ester, was firstly synthesized in 1849, little is known about its stability and decomposition reactions under severe thermal conditions. In the U.S., ETN has become a material of concern because the precursors are readily obtained and nitration with mixed acid is relatively straightforward.[1] Thus, there is a prompt need in acquiring a thorough understanding of its detonation characteristics and chemistry of decomposition.2[,3,4] Because ETN has the same number of nitro groups and better oxygen balance than Pentaerythritol tetranitrate (PETN), we have examined it for possible replacement of PETN in formulations.[5] However, its low melting point (60°C) requires that its thermal stability be

carefully examined. The current study employed both experimental and computational methods to investigate the thermal stability of ETN under thermal decomposition conditions. Isothermal aging was employed to provide an assessment of thermal kinetic parameters. Decomposition products were analyzed using mass spectrometry (MS) to determine if ETN decomposition is similar to PETN. In addition, Density Functional Theory (DFT) calculations at the B3LYP/6-311G(d,p) level of theory were used to characterize the decomposition mechanisms of ETN in the gas phase. To supplement the gas phase calculations, reactive molecular dynamics simulations with the ReaxFF-*lg* force field augmented with the DFT calculations of the major decomposition routes, were conducted to reveal the decomposition mechanisms operating at the reaction zone under simulated detonation conditions.

Experimental Section

Materials

ETN was prepared by nitration with acetyl nitrate, a route which results in a high yield of product more completely nitrated than by the mixed acid method.[6] Glacial acetic acid (16.7 mL) and acetic anhydride (16.7 mL) was added to a round bottom flask and suspended in an ice bath. White fuming nitric acid (8.4 mL, 99%) was added dropwise maintaining a reaction temperature below 10 °C. The reaction mixture was allowed to stir for 30 minutes; then meso-erythritol (2 g) was added portion wise keeping the temperature below 10 °C. This mixture was allowed to stir for 2 hours at 0 °C before it was removed from the ice bath and stirred another 2 hours at room temperature. The reaction mixture was poured into a beaker of ice water, filtered, rinsed with copious amount of ice water, and allowed to dry. The crude product (4.54 g) was recrystallized from isopropanol and filtered to give the pure product (3.90 g). Purity was checked by melting point and liquid chromatography/mass spectrometry detector (LC-MS).

Our experiments also required crude, partially nitrated ETN. Since mixed acid nitration generally produces less complete nitration, this method was used with slight modifications.[7] Sulfuric acid (3.0 mL, 96.5%) was added to a round bottom flask and cooled to 0 °C. White fuming nitric acid (4.6 mL, 99%) was added dropwise maintaining a reaction temperature below 10 °C. The mixture was allowed to stir for 30 minutes at 0 °C, and erythritol (1 g) was added portion wise keeping the temperature below 10 °C. This mixture was allowed to stir one hour at 0 °C rather than 30 °C. The nitration mixture was also not allowed to stand for an additional half hour; instead it was precipitated in a beaker of ice water and neutralized with sodium

bicarbonate. The resultant crude product was filtered, rinsed with ice water, and allowed to dry. It was not recrystallized. Figure 1 shows the nitration of erythritol to ETN.

IR, Raman, and NMR Spectra

IR spectra of solid ETN was obtained on a Thermo Scientific FTIR Nicolet 6700 ATR IR. Raman spectra of solid ETN were obtained using an Ondax 785.4 nm 225 mW laser and an Andor Shamrock 500i- D2-R spectrometer. The "Step and Glue" function was used, allowing the spectrometer to focus on a 2000 pixel portion of the spectrum at a time, and then assemble a continuous spectrums. Each spectrum is a summation of ten spectra each with one second exposure time. The spectral range was from 755 nm to 1040 nm. The grating of the spectrometer was set to 1200 lines/mm and a blaze of 850.

One proton NMR sample was prepared by dissolving ETN in deuterated chloroform. The spectrum was collected on a Brüker Ultrashield 300 with a frequency of 300.13 MHz, a sweep width of 6188.199 Hz, a center of 1853.43 Hz, calibrated on TMS at 0 ppm in deuterated chloroform ($CDCl_3$) using the pulse program zg30, a 1D pulse program with a 30° flip angle, using 16 scans and 2 dummy scans.

A second proton NMR sample was prepared by dissolving ETN in deuterated acetone. The spectrum was collected on a JEOL Eclipse Fourier Transform Nuclear Magnetic Resonance Spectrometer equipped with a 400Mhz Oxford liquid refrigerant cooled superconducting magnet with a frequency of 400.13 MHz, a sweep width of 8802.55 Hz, a center of 513.5938 Hz, calibrated on acetone at 2.09 ppm in deuterated acetone using the pulse program zg30, a 1D pulse program with a 30° flip angle, using 17 scans.

Carbon NMR samples were prepared by dissolving ETN in dimethylsulfoxide (DMSO). Sample was run on a JEOL Eclipse Fourier Transform Nuclear Magnetic Resonance Spectrometer equipped with a 400MHz Oxford liquid refrigerant cooled superconducting magnet, multinuclear tunable probe with temperature control and gradient shims. Carbon spectra were acquired using a decoupled single pulse and signal averaged over 1000 scans.

Kinetics

Samples were quantified using a liquid chromatograph on a 2.1x50 mm, 3 μm, 120 Å, Acclaim™ Polar Advantage II C18 (PA2) column coupled to a Thermo Electron Quantiva triple quadrupole mass spectrometer (LC-MS) with a heated electrospray ionization (HESI) source.

Conditions for HESI analysis were: negative ion spray voltage 2800 V; sheath gas 65 AU; auxiliary gas 15 AU; sweep gas 2 AU; ion transfer tube 250 ºC; and vaporizer temperature was 220 ºC. Data collection and analysis was performed with Thermo Xcalibur software version 2.2, SP 1.48. LC solvent flow was composed of water with 200µM ammonium chloride, 200µM ammonium acetate, and 0.1% formic acid (A); and acetonitrile (B). The solvent flow rate was 300 µL/min with the following gradient program (A%-B%): 0 to 1 min isocratic 70%-30%, 1 to 4 min gradient from 70%-30% to 5%-95%, 4 to 5.5 min isocratic 5%-95%, 5.5 to 6 min gradient from 5%-95% to 70%-30%, 6 to 7 min isocratic 70%-30%. Methanol (MeOH), acetonitrile (ACN), and water (H_2O) used to prepare samples and for all LC-MS work was Optima™ LC-MS Grade.

ETN (1.000mg +/- 0.050mg) was added to melting point capillaries, which were then sealed with a flame sealer. Sealed capillaries were placed in a sand bath in an oven and aged isothermally for various time intervals. The capillaries were broken into vials containing 20.0 mL of methanol. The vials were placed on a shaker for 1 hour and sonicated for 1 hour. The resulting solution was syringe filtered to remove any glass particles. These samples were diluted (100 µL sample, 0.9 mL ACN:H_2O 50:50 v:v) into LC vials. An internal standard (0.05mL of 5µg/mL 2,4-dichlorophenoxyacetic acid in ACN:H_2O) was added to each LC vial. ETN standards were prepared in ACN:H_2O at concentrations of 1, 2, 3, 4, 5, and 6 µg/mL. 1.0 mL of each standard was added to LC vials and spiked with the same quantity of the internal standard as the samples. Standards and samples were run using the LC-MS method described above and quantified based on the area under the chromatogram curves for ETN (retention time = 3.9 min).

For ETN in benzene the thermolysis process described for neat ETN was used with slight alterations in samples preparation. Stock solutions of ETN in benzene were prepared (100 +/- 10 µg/mL ETN) and ampules were charged with 1.0 mL of stock solution then sealed. Ampules were cooled in liquid nitrogen to solidify the benzene before being flame sealed using a propane-oxygen torch. Following thermal aging, ampules were broken into empty vials. Since the benzene was not miscible with ACN:H2O the vials were then placed on an Organomation N-EVAP 116 nitrogen evaporator to remove the benzene. Once the vials were dry 20.0 mL of ACN:H_2O was pipeted into the vials. The vials were placed on a shaker for 1 hour and sonicated for 1 hour. The resulting solution was syringe filtered to remove any glass particles. 1.00 mL of the filtered solution was added to LC vials, no additional dilution was necessary. An internal

standard (0.05mL of 5μg/mL 2,4-dichlorophenoxyacetic acid in ACN:H_2O) was added to each LC vial. Samples were run using the LC-MS method described above and quantified based on the area under the chromatogram curves for ETN.

Plotting the natural logarithm of fraction ETN remaining versus heating time in seconds (s) allowed determination of the rate constant k (s^{-1}) at each temperature from the slope (Table 1). Plotting natural log of rate constant against -1/RT, (where R = 0.00831 kJ/K●mol; and T, temperature in Kelvin) gave a slope with activation energy, Ea, (kJ/mol) and y-intercept of natural log of the pre-exponential factor, A (s^{-1}).

Product Analysis

To identify potential decomposition products, partially decomposed samples were reexamined by LC-MS under different conditions than were used in the kinetics studies. These partially decomposed samples, representing 10-25% decomposition, produced at various temperatures, were run on the Quantiva LC-MS using a precursor ion scan. The mobile phase gradient, column, and ion source parameters were the same as for the quantification method described in the kinetics experimental section. To scan for decomposition products a precursor ion scan was set to look for precursor ions that fragmented into ions with m/z 62 (NO_3^-) and 46 (NO_2). The first quadrupole was set to allow ions with m/z 80-800 through one m/z at a time. Each ion was then fragmented in the second quadrupole using argon collision gas at 1.5 mTorr with a collision energy ramp from 10 to 20 V. The third quadrupole scanned for anything that created fragments of m/z 62 and 46. The resulting chromatograms showed what parent ions in the decomposition products generated these fragments.

The partially decomposed samples were also run on a Thermo Exactive Orbitrap High Resolution Mass Spectrometer with an Atmospheric Pressure Chemical Ionization (APCI) source coupled to an LC, using the same LC parameters as on the Quantiva. Conditions for APCI analysis were: sheath gas 35 AU; auxiliary gas 17 AU; sweep gas 0 AU; discharge current 10 μA; capillary temperature 150 ºC; capillary voltage -25.00 V; tube lens voltage -100.00 V; skimmer voltage -18.00V; and vaporizer temperature was 200 ºC . The Orbitrap MS was set to negative mode, high resolution (50,000), 50 ms maximum inject time, and looked for ions m/z 100-1000. The resultant data was analyzed by generating extracted ion chromatograms for the exact mass of potential decomposition products (m/z +/- 5 ppm) of ETN (Table 3).

Decomposition product chromatograms were compared to crude, non-fully nitrated ETN chromatograms to verify some of the products.

Computational Details

DFT calculations

The quantum chemical calculations were carried out using the Gaussian-09 package[8]. The B3LYP hybrid density functional[9] was used in conjunction with the Pople triple ξ (6-311G) basis set. The energetics for local minima and transitions states was recalculated using augmented diffuse functions (6-311G++(d,p)) basis set. Relative energy of proposed chemical reactions include the zero-point energy (ZPE) correction of the corresponding species. All the calculated frequencies, the zero point energies and the thermal energies correspond to harmonic approximation. The calculations of intrinsic reaction coordinates (IRC) using internal coordinates were performed in order to examine whether the transition states under consideration connect the expected reactants and products.

ReaxFF-lg Thermal Decomposition Simulations

The computational cell of crystalline ETN contained 256 molecules (6656 atoms) and was created by multiplying each one of the $\vec{a}$, $\vec{b}$ and $\vec{c}$ unit cell vectors by 4. The resulting super-cell had dimensions: 63.8Å×20.8Å×52.9Å with monoclinic symmetry. Minimization of potential energy was carried out using a conjugate gradient algorithm, followed by temperature (NVT) and pressure (NPT) equilibration steps at ambient conditions (300K and 1atm) for 10ps each. The calculated bulk density of the equilibrated sample was d_0=1.78±0.01 gr/cm^3, in excellent agreement with experiment (1.773 gr/cm^3 at room temperature). Thermal decomposition simulations at simulated detonation conditions (T_{CJ}=4300K, P_{CJ}=26GPa) were carried out in the NPT ensemble. During the simulations, bond orders between each pair of atoms were monitored and properly averaged to avoid identification of artificial covalent bonds during possible short-lived, high energy encounters of two atoms. The ReaxFF-*lg* force field used in the study was further augmented with the reported DFT calculations of unimolecular and bimolecular decomposition energy barriers. The resulting force field accurately reproduced the major decomposition channels of ETN as can be seen in the supplementary information (SI 1).

Results & Discussion

Kinetics

We have previously compared the rate of decomposition of ETN and PETN by differential scanning calorimetry (DSC); ETN appeared to decompose more rapidly. Figure 2 illustrates this. To assign reliable values to the ETN decomposition, isothermal studies were performed on neat ETN over the temperature range 60 to 140ºC. In one set of experiments ETN (100 ug/mL) was heated in benzene at 80ºC; under these conditions ETN decomposed somewhat slower than observed in the condensed phase (Table 1). Percent ETN remaining was assessed from liquid chromatography; only in a few instances did any ETN survive past 70-75% remaining. Sample decomposition tended to accelerate rapidly from 25-30% decomposition to 100% decomposition. This autocatalytic decomposition can be attributed to the reactive nature of ETN as well as that of its decomposition products (discussed in next section).

Rate constants (k in s^{-1}) at each temperature were determined and plotted in Arrhenius fashion. The Arrhenius parameters are listed in Table 2. Figure 3 shows the Arrhenius plots generated from our isothermal ETN decomposition data as well as that of German[10] for PETN. The rest of the lines have been generated from reported Arrhenius parameters.[6,11,12] The isothermal ETN data overlaps with Roth's[11] values for PETN, but Roth's reported kinetics are significantly faster than both those of Robertson[12] and of German.[10] Robertson reported Arrhenius parameters for the decomposition of neat PETN and in dicyclohexyl phthalate solution. He observed a slight deceleration of the decomposition in solution, and in the present study a similar retarding of decomposition was observed when ETN was heated in benzene. The preponderance of data suggests ETN decomposes faster than PETN. This is not surprising since ETN melts at much lower temperature than PETN, and many explosives decompose immediately upon melting. However, from its DSC trace, ETN appears to have a wider temperature stability range than PETN (Fig. 2); like TNT, its decomposition does not immediately follow its melt. Elsewhere we have reported our attempts to exploit this feature.[5]

It is generally accepted that "the decomposition of primary and secondary aliphatic nitrate esters involves the initial, reversible, rate determining scission of the O-NO_2 bond" (Figure 4).[13,14,18] This is expected to be the first step in ETN decomposition, as well. However, unlike in PETN, the nitro groups in ETN are not all equivalent. DFT calculations and ReaxFF-*lg*

reactive molecular dynamics simulations together with experimental product analysis were performed to probe ETN decomposition routes.

Product Analysis

The LC-MS Quantiva precursor ion scan showed only two parent ions which produced m/z fragments of 62 (NO_3^-)--ETN and erythritol trinitrate $C_4H_7N_3O_{10}$ (EtriN). Under the fragmentation conditions, no parent ions were found to produce fragment m/z of 46 (NO_2^-). The LC-MS Orbitrap found additional evidence of decomposition products erythritol dinitrate $C_4H_8N_2O_8$ (EdiN) and erythritol mononitrate $C_4H_9N_1O_6$ (EmonoN). These may not have been observed in the Quantiva because either they did not produce a m/z fragment of 62 or, more likely, the Orbitrap was simply more sensitive to the mono and di-nitrated species, especially when using an extracted ion chromatogram. The increased resolution of the Orbitrap allowed examination of an extracted ion chromatogram in a mass window of less than 0.005 amu. This reduced background signal to almost nothing since, for small molecules, the only interfering ions would be those with identical chemical formulas as the analyte. LC-MS extracted ion chromatograms and mass spectra are included in supplemental information (SI 2-4).

Density Functional Theory (DFT) calculations were performed to assess and compare potential first-steps in the PETN and ETN decompositions. Two possible unimolecular decompositions were considered (Figures 5, 6). Breaking the O-NO_2 bond would form two radicals --$\cdot NO_2$ and the rest of molecule. This reaction proceeds via a transition state for which the energy barrier is approximately the same as the energy of reaction. It corresponds to bond dissociation energy. Subsequent reactions would involve ejection of other radicals, and these would proceed via low energy barriers. With free $\cdot NO_2$ in the formulation, autocatalytic decomposition would be expected. The exothermic ejection of HONO was also considered as a potential first-step in decomposition. For ETN decomposition, creation of two radicals by elimination of $\cdot NO_2$ proceeds via an energy barrier about 37 (30) kJ/mol lower than elimination of HONO, where the elimination of internal groups requires less energy in both reactions. This route is more favored than it is for PETN. In PETN, HONO elimination proceeds via an energy barrier only slightly higher than the decomposition path forming two radicals by about 10 kJ/mol. Unlike PETN, the carbons in ETN are inequivalent. The O–N bond energy in CH_2O–NO_2 (terminal C) and CHO–NO_2 (internal C) differ. Computed energy level diagrams show that $\cdot NO_2$ elimination is favored from the internal carbon (Figure 6). Computation also reveals that

potential bimolecular H-atom migration between two PETN or ETN molecules is unfavorable (Figures 5 and 7). The lack of bimolecular ETN decomposition is supported by the observation that the rate of ETN decomposition at 80ºC remained essentially identical whether performed neat or in benzene solution (Table 1). This result also agrees with a recent theoretical study of thermal decomposition of condensed phase energetic materials18.[18]

To shed light on the initial steps of thermal decomposition of bulk ETN in a detonation scenario, reactive molecular dynamics simulations were performed on a model single crystal of ETN. The ReaxFF-*lg* force field that was previously trained to accurately reproduce reaction energetics and equations of state of energetic materials22, including PETN, was used in the simulations. We have augmented the force field with additional DFT data related to ETN, including molecular structures, partial atomic charges and main decomposition reactions reported in this study, to obtain a high quality force field for ETN chemistry under ambient and extreme conditions. Thermal decomposition simulations were performed in a constant pressure ensemble (NPT) at 4300K and 26GPa simulating the Chapman-Jouguet point. Figure 8 presents the initial steps of ETN decomposition as a function of time under these conditions. The results clearly show that the decomposition sequence begins with the cleavage of the O-NO_2 bond, the weakest bond in the molecule. This leads to increasing concentration of $\cdot NO_2$ radicals in the system, reaching a peak value of 1.2 times that of the initial amount of ETN molecules after about 1.8ps. Concurrently, the trinitrate (EtiN), dinitrate (EdiN) and mononitrate (EmoN) forms of ETN are observed pertaining for subsequent cleavage reactions. These species were also experimentally observed in the LC-MS Orbitrap measurements and in a recent study of shock induced decomposition of ETN2.[2] The $\cdot NO_2$ radicals quickly (~2ps) disappear forming more stable nitro intermediates. A known competing reaction to the O-NO2 cleavage in nitro esters is the elimination of HONO (nitrous acid) as is observed in the DFT calculations. This reaction requires overcoming a barrier of 136.0 kJ/mol or 158.2 kJ/mol for an internal or external elimination, respectively. Accordingly, the formation of HONO slightly lags behind and is a less favorable route (Figure 8). Nevertheless, contrary to $\cdot NO_2$ elimination which is purely endothermic, the formation of HONO releases 130.1 kJ/mol and 164.0 kJ/mol of energy for the internal and external cleavages, respectively. Hence, this route could lead to an almost self-sustained propagation of decomposition. The ·NO is another radical species reaching a significant amount during the initial stages of ETN decomposition. This species appears when

ETN relative amount in the system is nearly 40%, hence it does not seem to be a trigger reaction for decomposition, but rather plays the role of a secondary byproduct. A possible route for the production of NO under the assumption of ground state decomposition is the bimolecular reaction, where RO· is an ETN moiety,

$$RO\cdot + \cdot NO_2 \rightarrow ROO\cdot + \cdot NO$$

It should be noted that ·NO has been detected experimentally in several thermal decomposition studies of PETN.[20,21] Formaldehyde is another intermediate observed during secondary products evolution under detonation conditions. It reaches a peak amount (20% relative to ETN) concurrently with HONO, but decays faster to negligible amounts. Other less significant intermediates during decomposition involve $\cdot NO_3$ and NO_xH_y and various carbon moieties of ETN at ow amounts, hence, they were not presented in Figure 8 for clarity.

The stable decomposition products of ETN are presented as a function of time in Figure 9. It can be inferred from the figure that a steady state in stable decomposition products concentrations is reached approximately after 10-20ps. However there is a clear distinction between the rates of formation of different stable products. The formation rate of H_2O is the highest and it is also the most abundant species. N_2 and CO_2 evolve at similar rates and reach practically identical final amounts. Minor products, including ·OH, H_2O_2 and trace amounts of H_3O_2 evolve at an intermediate rate. CO is not formed at all since ETN bears a positive oxygen balance of 5.3%. Thus, the net decomposition reaction occurring in the reaction zone of a detonation wave can be summarized as follows:

$$C_4H_6O_{12}N_4 \rightarrow 1.4CO_2 + 1.5H_2O + 1.4N_2 + (0.3OH + 0.2H_2O_2)$$

Detailed analysis of the carbon distribution in the system revealed no apparent formation of carbonaceous clusters due to incomplete oxidation reactions. The initial carbon in the system resides solely in the ETN molecules, hence the average number of carbon atoms per molecule is 4, as can be inferred from the left panel in Figure 10. Accordingly, the ratio of carbon atoms out of total number of atoms in the molecules is 4/26≈15.3%. During the very first endothermic stage of decomposition, covalent bonds begin to break, and the initial intermediates are highly transient carbonaceous radicals including covalent dimers. Interestingly, the relative amount of carbon atoms in these species grows rapidly during the first 1.7ps and then gradually decreases to

a steady state value of ~24%. This trend parallels the instantaneous increase in the average number of carbon atoms in each species and the rapid fall off to an approximate value of 1.5 carbon atoms per species at later times. To understand the underlying mechanisms of carbon transformation in the system, elemental analysis was performed on all carbonaceous species in the system. This is shown in the right panel in Figure 10. The initial elemental ratios correspond to the expected ratios in ETN molecule and the rapid fall off marks the commencement of the decomposition process. However, unlike the N/C and H/C ratios which continue to gradually decrease, the O/C ratio rises rather quickly to its steady state value. Evidently, the rise in the relative amount of oxygen atoms compared to carbon atoms is due to various oxidation processes. These can be divided into three regimes: instantaneous bond breaking (0ps until 1.7ps), fast oxidation (from 1.7ps until 7.0ps) and a slow oxidation regime (from 7.0ps onwards). The transition between the first and the second stages coincides with the time of complete decomposition of the initial ETN molecules (Figure 8). Thus, the first stage represents the initial degradation mechanisms of parent ETN molecules, mainly via the release of $–NO_2$ and $-ONO_2$ groups. The second, intermediate stage, is governed by the rapid oxidation of unstable intermediates, while the third, slow stage originates from the oxidation of less reactive species coupled to the diffusion mechanisms of free oxygen and other oxidizing agents in the system. At the end of 60ps of decomposition, approximately ~3% of molecular oxygen is still present in the system. Clearly, the simulation duration is not enough for these slow oxidation processes to reach full chemical equilibrium. Nevertheless, the slight gradual increase in O/C ratio indicates that such a state shall indeed be reached. Counter intuitively, the O/C ratio is slightly higher than 2 which would be expected in the state of a complete combustion. This is due to the formation of several over-oxidized species, such as CO_3, C_2O_4 (CO_2 dimer) and C_2O_4-H radicals. In addition, the final average number of carbon atoms per molecule (Figure 10, left panel) is around 1.5, rather than 1.0, indicative of covalent dimers. However, their amounts in the system are quite low and these highly unstable species will eventually disintegrate into the thermodynamically stable CO_2 under isentropic cooling following the expansion of the detonation products on much longer timescales.

Table 4 compares the energies involved in various decomposition routes of PETN and of ETN. The energy differences for the elimination reactions between ETN and PETN are not large; both can access NO_2 or HONO elimination routes. The main difference between the two nitrate

esters is in H-interexchange reaction, in which ETN can transfer an internal H at lower energy cost than PETN[16,17]. However, such a reaction would be expected to form a strong carbonyl bond along with NO_2 ejection. This is not observed under the present experimental conditions.

The decomposition products observed by LC-MS were derivatives of ETN in which, to some extent, CO-NO_2 had been replaced by CO-H, reforming the tri-, di-, and mono- nitrate esters of erythritol. To assess whether H-transfer had formed ketone or aldehyde groups (Figure 7) which had been transformed into alcohol species during the experimental workup, partially nitrated erythritol was prepared as described in the Experimental Section. On the Orbitrap LC-MS, extracted ion chromatogram monitoring of m/z 291.9825 detected three peaks (Figure 11a). The peak at retention time 4.09 min was assigned to ETN, that at 3.54 min to erythritol trinitrate, and the small peak at 3.36 min may also be trinitrate which was nitrated on different carbons. Extracted ion chromatograms were also generated for m/z 246.9975 and m/z 202.0124, looking for evidence of erythritol dinitrate and mononitrate, respectively. Only the tetra- and tri-nitrates were observed. The 291.9825 m/z extracted ion chromatogram was compared to that of pure ETN which had been partially decomposed (Figure 11b). Two peaks were observed corresponding to the undecomposed ETN (retention time = 4.09) and the trinitrate (retention time = 3.54). The retention time for the erythritol trinitrate matched the largest trinitrate peak in the crude material. Thus, the main decomposition product was erythritol trinitrate, in which an alcohol group replaced one nitrate and that alcohol was an original decomposition product of ETN, not a product of subsequent analytical workup. The chromatograms of the partially decomposed ETN were searched for additional products, including the ketone and polymerized ETN. Structures searched are shown in Table 3; no decomposition products other than the lesser nitrates were discovered. In well-sealed and highly decomposed samples, red gas, assumed to be NO_2, was observed. This generation of NO_2 from ETN would explain the auto-catalytic decomposition observed in ETN kinetics experiments.

We have previously reported the infrared and Raman spectra of ETN.[6] Theoretical computations now permit assignment of major features. Figure 12 shows three major IR peaks assigned as ONO scissoring, symmetric NO_2 stretching, and asymmetric NO_2 stretching. In Raman spectra three major peaks are assigned as OCH rocking, NO_2 scissoring, and NO_2 symmetric stretching (Figure 13). The ^{1}H decoupled ^{13}C NMR in DMSO showed two singlets-terminal C at 68.7 and internal C at 76.5 ppm, which compares well to ETN in $CDCl_3$ with

terminal C 74.9 and internal C 67.4 ppm reported by Matyas[19] (Figure 14). Proton NMR of ETN was performed in acetone and $CDCl_3$. In $CDCl_3$ four doublets were observed at 4.65, 4.69, 4.91, and 4.96 ppm representing the four protons on the terminal carbons. A multiplet at 5.51 ppm corresponded to the two protons on the internal carbons. Acetone proton NMR was similar with four doublets observed at 5.01, 5.05, 5.25, and 5.29 as well as a multiplet at 6.04 (Figure 15).

Conclusions

Experimental and computational study of ETN stability and reactivity in different thermal regimes was performed. Isothermal aging of ETN samples has provided insight into the thermal stability of ETN as well as details on the resulting decomposition products. Despite the ability to exist in a molten state, ETN has a lower thermal stability than its counterpart PETN. However, it was found that ETN was significantly more stable than estimated from DSC data.[3] Decomposition products identified were exclusively formed by loss of NO_2 which is often the case for nitrate esters. DFT computations indicated that the first step in ETN and PETN decomposition could be NO_2 or HONO ejection, though the former is more energetically favored. After the first step a number of decomposition routes become available. Reactive molecular dynamics revealed the initial steps of the decomposition mechanism at the CJ point of P_{CJ}=26GPa and T_{CJ}=4300K. At these conditions, it was observed that bulk ETN begins its decomposition by successively releasing $\cdot NO_2$ groups from parent molecules and that HONO elimination is a secondary reaction. The identified stable decomposition products are H_2O, CO_2 and N_2, where H_2O is the most abundant species in the hot and compressed state. No carbonaceous clusters were formed during decomposition since ETN should reach a complete oxidation. Furthermore, oxidation of carbon was observed to proceed in three steps. In the first stage ETN molecules undergo homolysis reactions to release $\cdot NO_2$ and $\cdot ONO_2$ groups. The second, intermediate stage, is governed by the rapid oxidation of unstable intermediates, while the third, slow stage originates from the diffusion of molecular oxygen and other oxidizing agents in the system. In experimental tests it was observed that ETN decomposition frequently accelerated rapidly beyond 25-30% to 100% decomposition; this can be explained by the reactive nature of the $\cdot NO_2$ radicals produced.

Acknowledgment

This material is based upon work supported by the U.S. Department of Homeland Security, Science and Technology Directorate, Office of University Programs, under Grant Award 2013-ST-061-ED0001. The views and conclusions contained in this document are those of the authors and should not be interpreted as necessarily representing the official policies, either expressed or implied, of the U.S. Department of Homeland Security.

References

1 Cook, M. Escondido: Authorities to burn "bomb factory" house http://www.sandiegouniontribune.com/news/2010/nov/30/escondido-authorities-to-burn-bomb-factory-house/.
2 Furman, D.; Kosloff, R.; Zeiri, Y. *J. Phys. Chem. C* **2016**, 120 (50), 28886-28893
3 Manner, V. W.; Preston, D. N.; Tappan, B. C.; Sanders, V. E.; Brown, G. W.; Hartline, E.; Jensen, B.; *Propellants, Explos. Pyrotech*. **2015**, 40, 460-462
4 Matyáš, R.; Künzel, M.; Růžička, A.; Knotek, P; Vodochodský, O. *Propellants, Explos. Pyrotech.* **2015**, 40, 185-188
5 Oxley, J. C.; Smith, J. L.; Brown, A. C. *Eutectics of Erythritol Tetranitrate*, submitted
6 Oxley, J. C.; Smith, J. L.; Brady, J. E.; Brown, A. C. *Propellants, Explos. Pyrotech.* **2012**, *37* (1), 24–39.
7 Ledgard, J. B. *The Preparatory Manual of Explosives*, 3rd ed.; 2007.
8 Frisch, M. J.; Trucks, G. W. Gaussian, Inc.: Wallingford, CT 2009.
9 Becke, A. D. *J. Phys. Chem.* **1993**, *98*, 5648–5652.
10 German, V. N.; Grebennikova, S. E.; Lobanova, S. P.; Fomicheva, L. V. *Int. Detonation Symp.* **2002**.
11 Fedoroff, B. T.; Sheffield, O. F. *Encyclopedia of Explosives and Related Items*; 1980; Vol. 8.
12 Robertson, A. J. B. *J. Soc. Chem. Ind.* **1948**, *67* (June), 221–224.
13 Roos, B. D.; Brill, T. B. *Combust. Flame* **2002**, *128* (1–2), 181–190.
14 Chambers, D.; Brackett, C.; Sparkman, O. *UCRLID-148956, July* **2002**.
15 Liu, W. G.; Zybin, S. V.; Dasgupta, S.; Klapotke, T. M.; Goddard, W. A. I. *J. Am. Chem. Soc.* **2009**, *131* (22), 7490–7491.
16 Chakraborty, D.; Muller, R. P.; Dasgupta, S.; Goddard, W. A. I. *J. Phys. Chem. A* **2000**, *104* (11), 2261–2272.
17 Wu, C. J.; Fried, L. E. *J. Phys. Chem. A* **1997**, *101* (46), 8675–8679.
18 Furman, D.; Kosloff, R.; Dubnikova, F.; Zybin, S. V.; Goddard W. A. III; Rom, N.; Hirshberg, B.; Zeiri, Y. *J. Am. Chem. Soc.* **2014**, 136, 4192-4200
19 Matyáš, R.; Lyčka, A.; Jirásko, R.; Jakový, Z.; Maixner, J.; Mišková, L.; Künzel, M. *J. Forensic Sci.* **2016**, *61* (3), 759–764.
20 Ng, W. L.; Field, J. E.; Hauser, H. M. *Journal of the Chemical Society, Perkin Transactions 2* **1976,** (6), 637-639
21 Ornellas, D. L.; Carpente.Jh; Gunn, S. R. *Rev Sci Instrum* **1966,** *37* (7), 907
22 Liu, L.; Liu, Y.; Zybin, S.V.; Sun, H.; Goddard, W.A. *J. Phys. Chem. A*, **2011**, 115 (40), 11016-11022

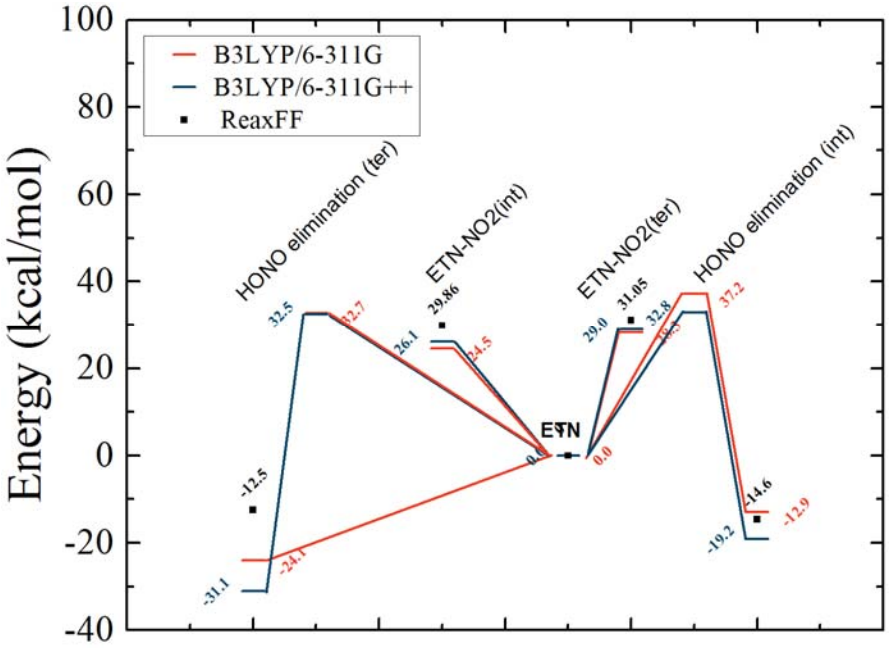

SI 1. Major unimolecular decomposition routes of ETN. Comparison between ReaxFF and DFT calculations.

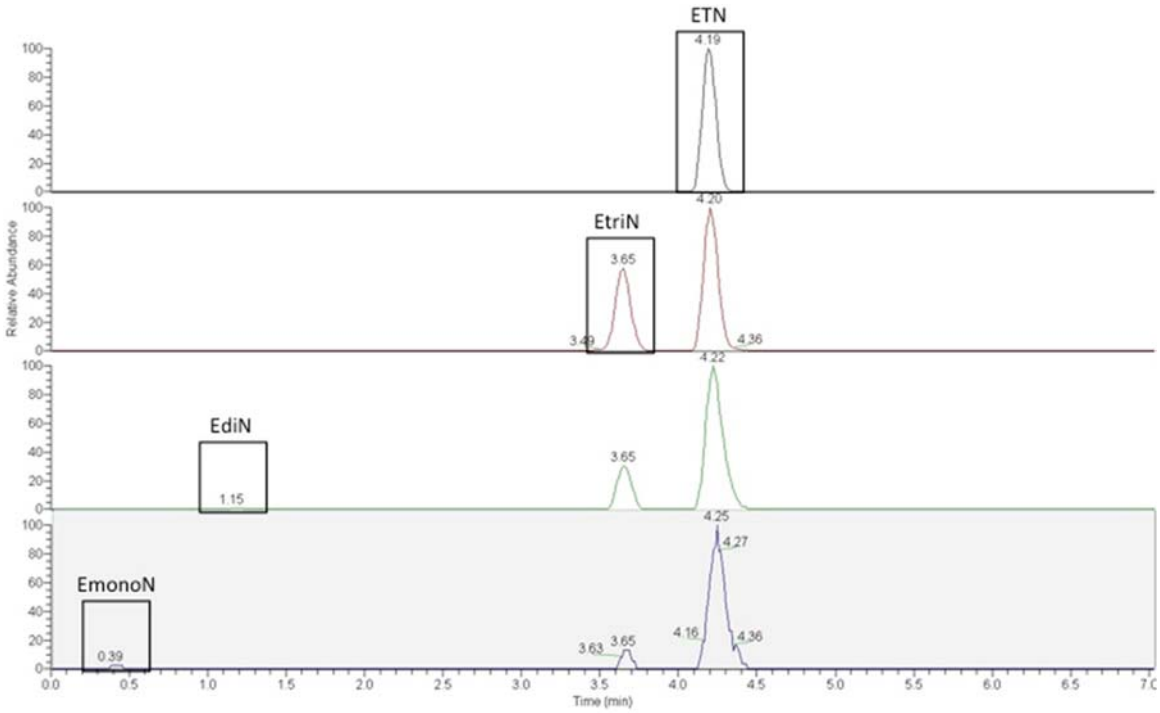

SI 2: Extracted ion chromatograms for ETN decomposition products: tetranitrate, trinitrate, dinitrate, mononitrate (top to bottom)

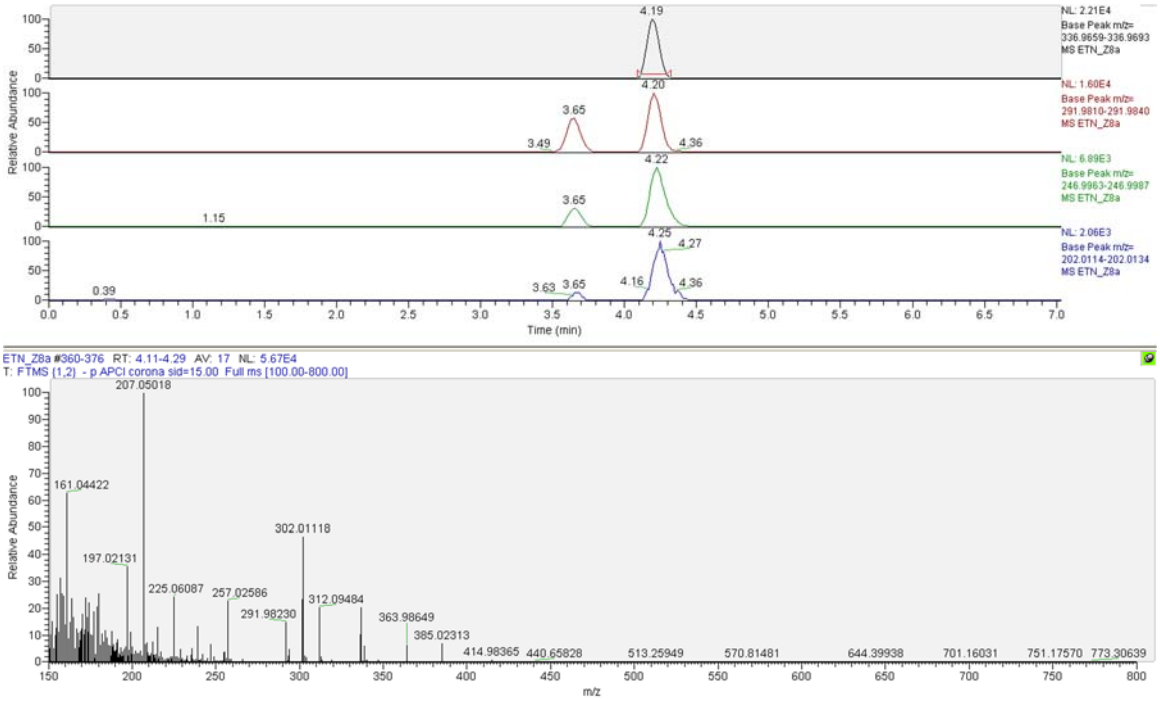

SI 3: Mass spec of ETN Peak

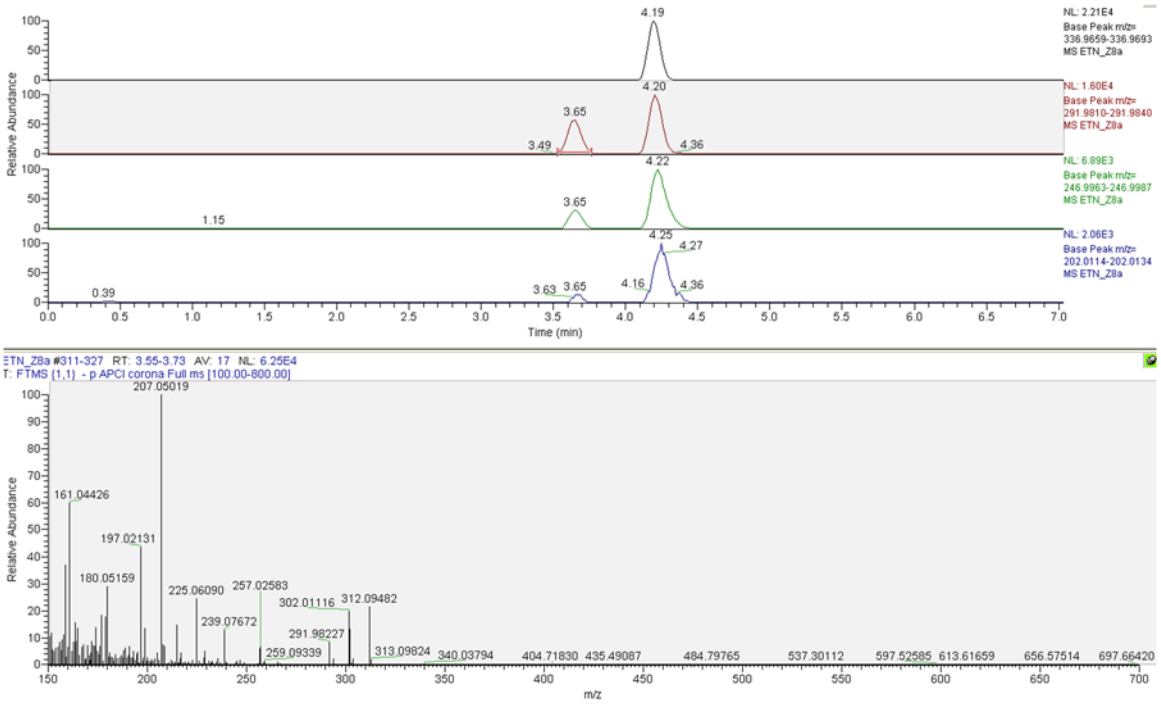

SI 4: Mass Spec of trinitrate peak, lowest nitrated compound mass spec that shows compound m/z above background without ion extraction.

List of Tables

Table 1: Table with ETN kinetics data both neat and in benzene.

T (°C)	1/RT (mol/kJ)	k (s^{-1})	ln(k)
60	0.361	1.48E-07	-15.7
80	0.341	1.47E-06	-13.4
80		9.80E-07	in benzene
110	0.314	3.12E-05	-10.4
120	0.306	4.51E-05	-10.0
140	0.291	2.14E-04	-8.45

Table 2: Arrhenius parameters for ETN and PETN

Compound	Method	Ea (kJ/mol)	A (s^{-1})	$k_{240°C}$ (s^{-1})	$k_{200°C}$ (s^{-1})	$k_{140°C}$ (s^{-1})	Ref.
ETN	Isothermal (LCMS)	104.3	3.72E+09	8.9E-02	1.1E-02	2.4E-04	This Work
ETN	DSC	95.0	2.35E+10	5.0E+00	7.5E-01	2.3E-02	3
PETN	Manometric	196.6	6.31E+19	5.9E-01	1.2E-02	8.4E-06	9
PETN	Monometric*	165.3	1.26E+16	1.9E-01	7.0E-03	1.6E-05	9
PETN	Weight Loss	161.5	1.58E+15	5.6E-02	2.3E-03	5.9E-06	8
PETN	Chemical Analysis	132.2	2.00E+13	6.8E-01	5.0E-02	3.8E-04	8
PETN	DSC	136.5	7.47E+14	9.4E+00	6.3E-01	4.0E-03	3
PETN	Manometric	217.4	4.70E+21	3.4E-01	4.6E-03	1.5E-06	7

* 5% in dicyclohexylphthalate

Table 3: Decomposition products searched for by high resolution LCMS

Found	Not Found
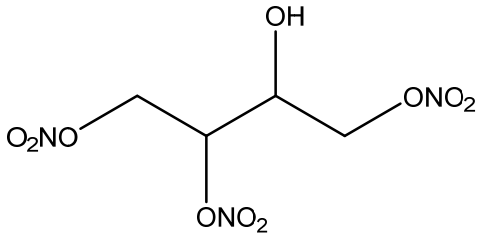	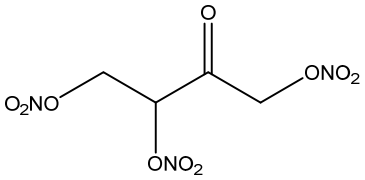
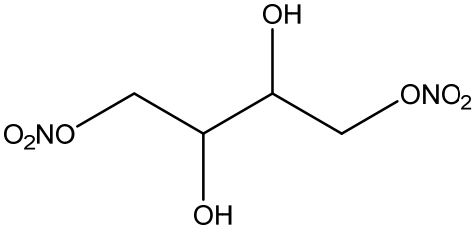	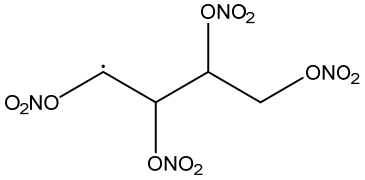
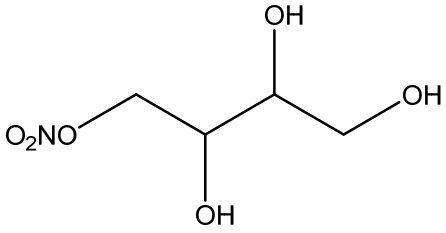	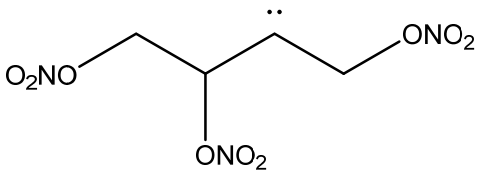
	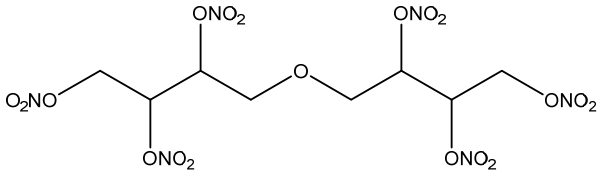

Table 4: Decomposition channels of ETN and PETN. Energy values in kJ/mol.
Method and basis set: B3LYP/6-311++G**.

Decomposition Reaction	ETN (lowest)	PETN
Elimination reactions		
+ NO_2 (radical) (BDE)	121.3 (109.2)	139.7 (163.2)[a]
+ HONO ($\Delta E^{\#}$)	158.3 (136.0)	149.8
+ HONO (ΔE_{react})	-164.0 (-130.1)	-92.0
H-atom transfer		
H-atom shift ($\Delta E^{\#}$)	172.4	
H-atom shift (ΔE_{react})	12.6	50.6

a. M06/6-311G** result from Liu, W.-G.; Zybin, S. V.; Dasgupta, S.; Klapotke, T.; Goddard W. III JACS, 2009, *131*, 7490 - 7491.

List of Figures

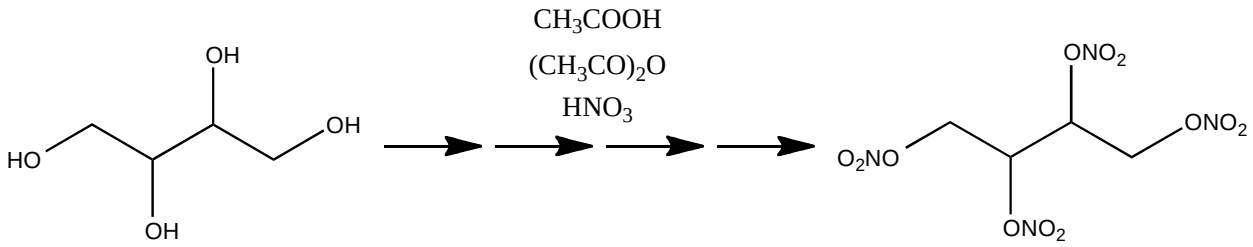

Figure 1: Nitration of erythritol to ETN, stepwise nitration of each alcohol

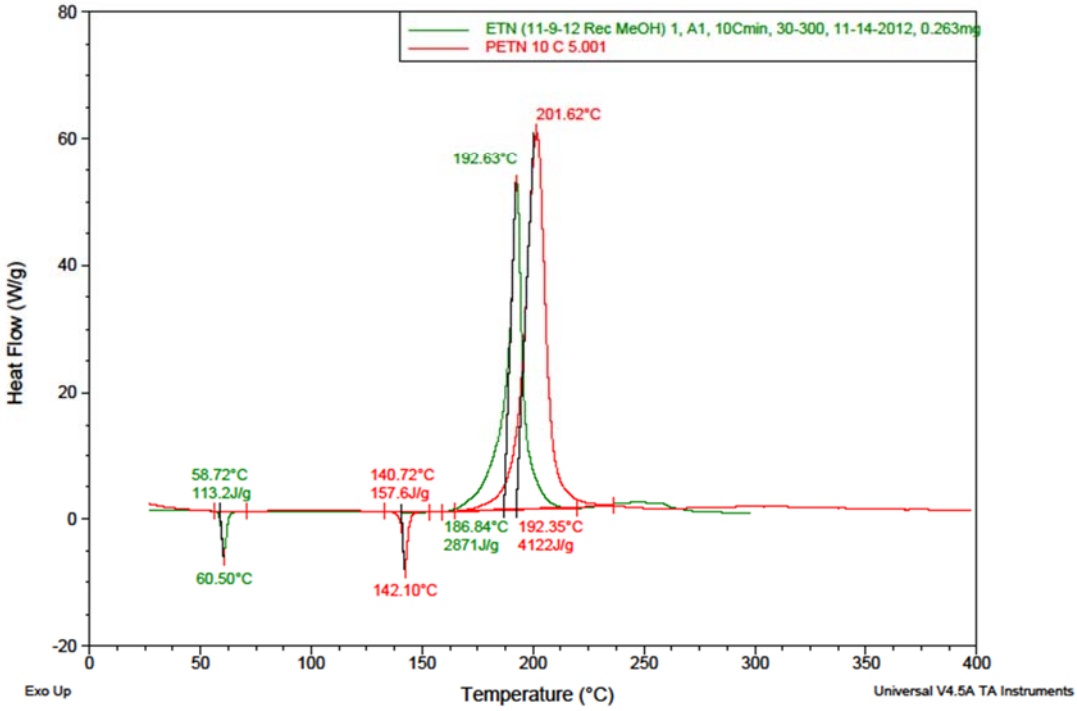

Figure 2: DSC overlay of ETN and PETN (10 °C/min)

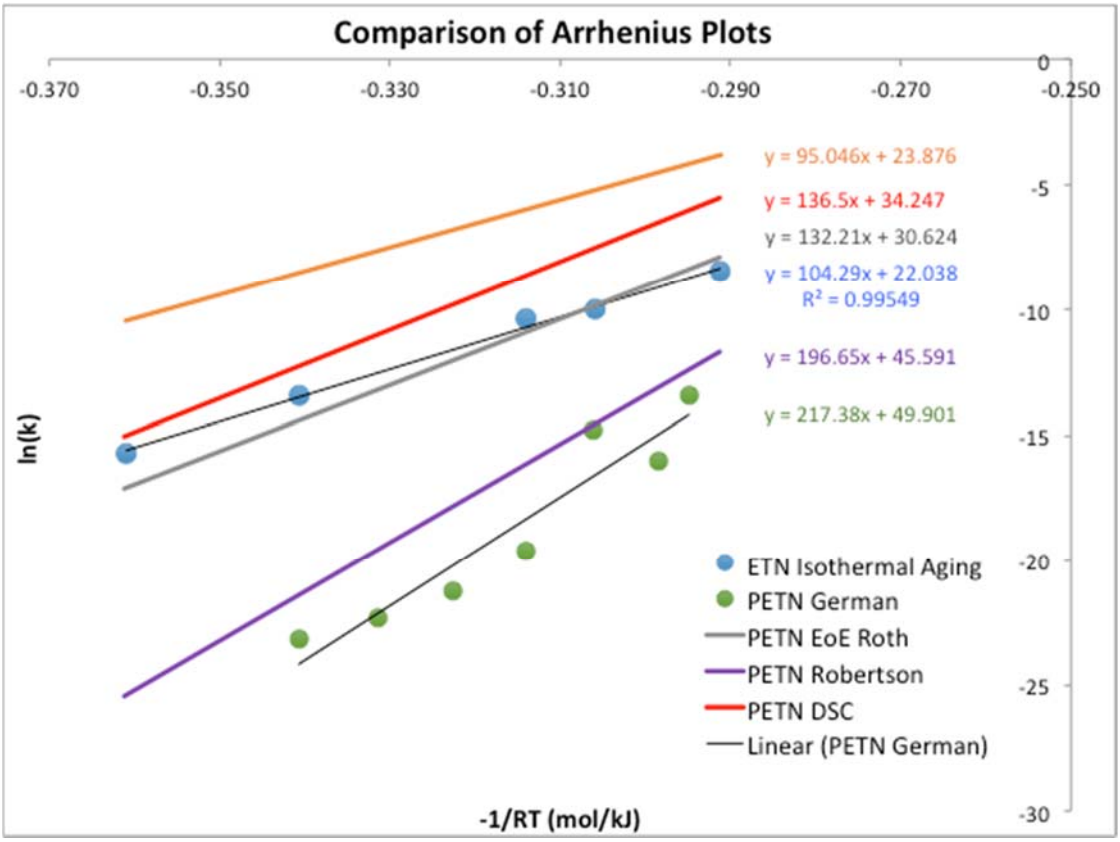

Figure 3: Arrhenius plots for ETN and PETN

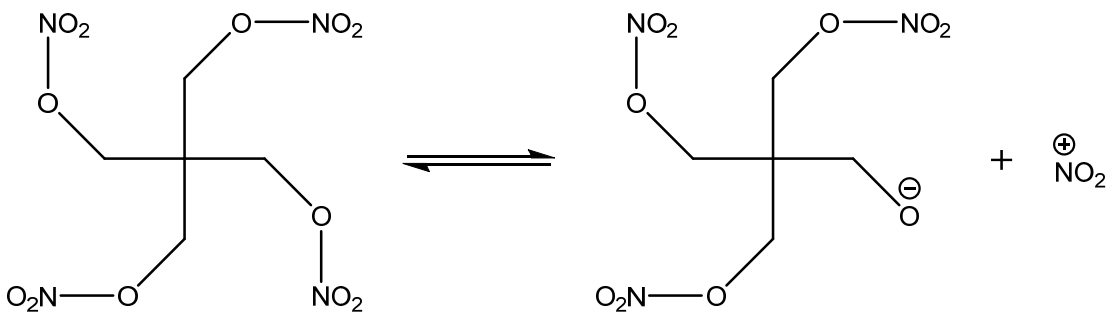

Figure 4: PETN loss of ·NO_2

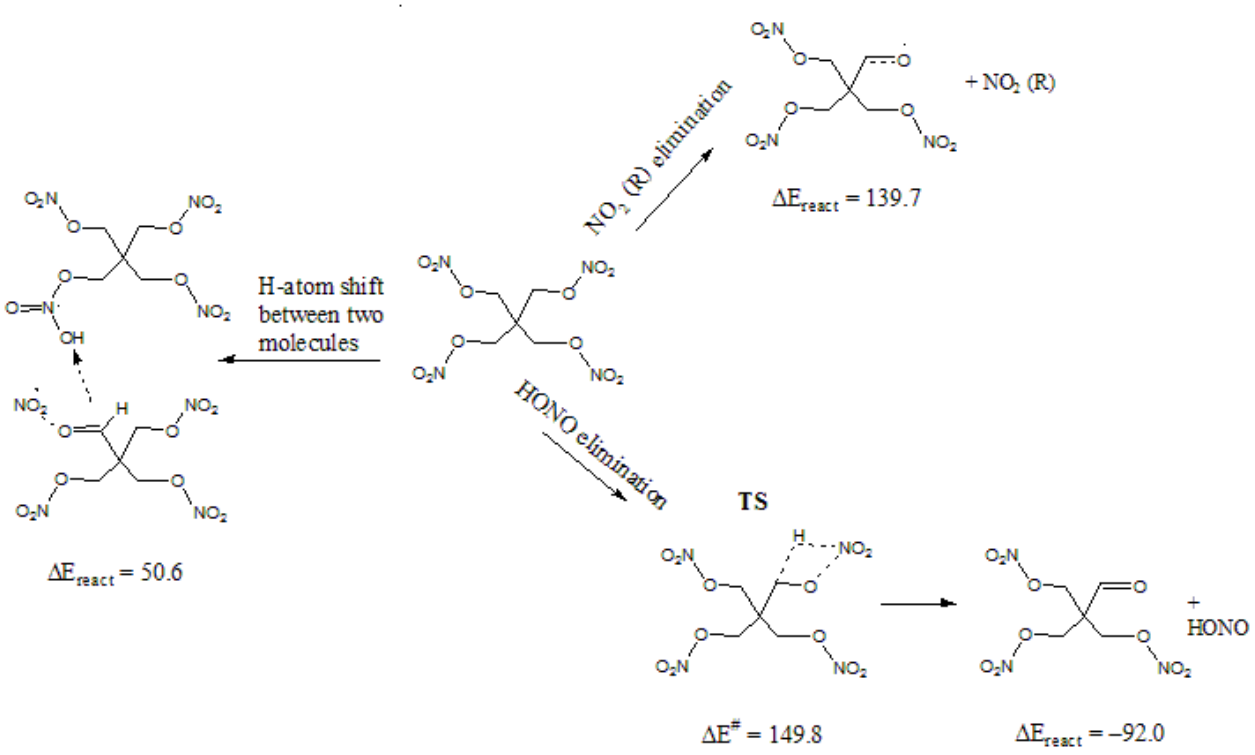

Figure 5: Energetics of PETN decomposition as calculated using B3LYP/6-311++G** level of theory. Energy values are given in kJ/mol.

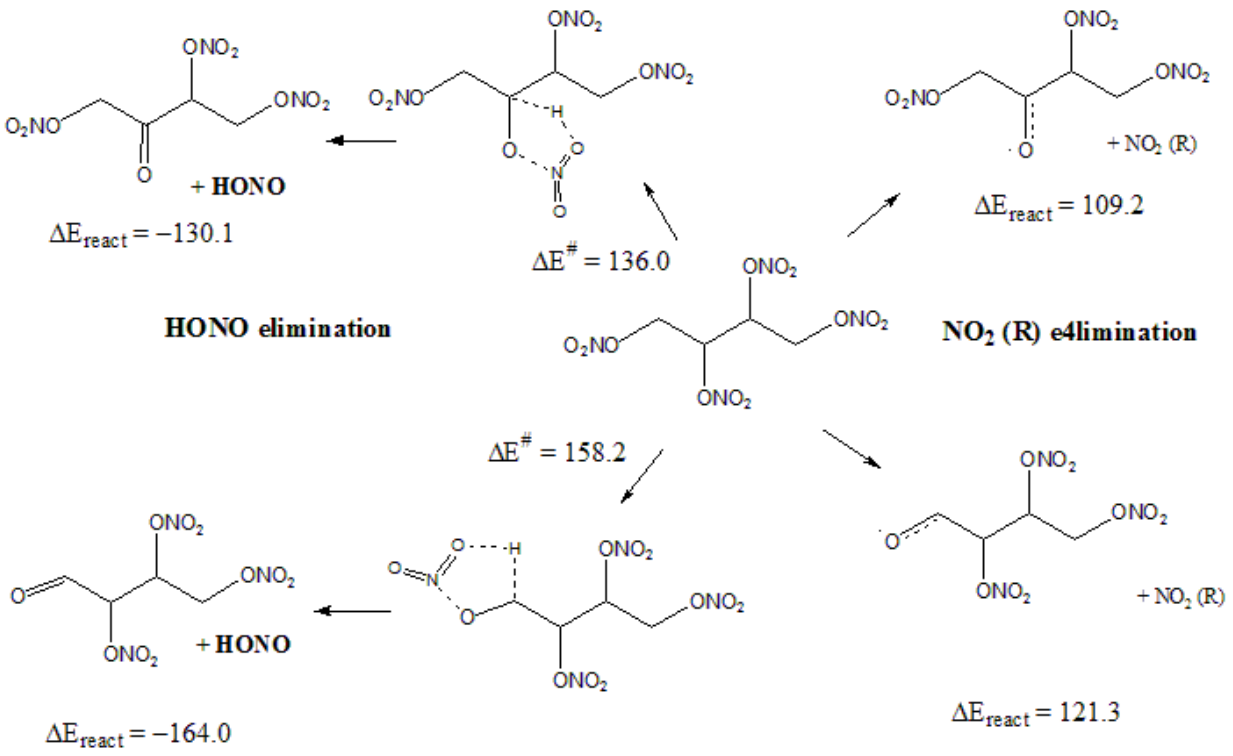

Figure 6: Energetics of ETN decomposition, calculated by B3LYP/6-311++G** level of theory. Top side of figure shows reactions in which ejection of $\cdot NO_2$ and HONO proceeds from the internal –CH-O-NO_2 group. Bottom side shows the same reactions proceed from the external –CH_2-O-NO_2 group. Energy values are given in kJ/mol.

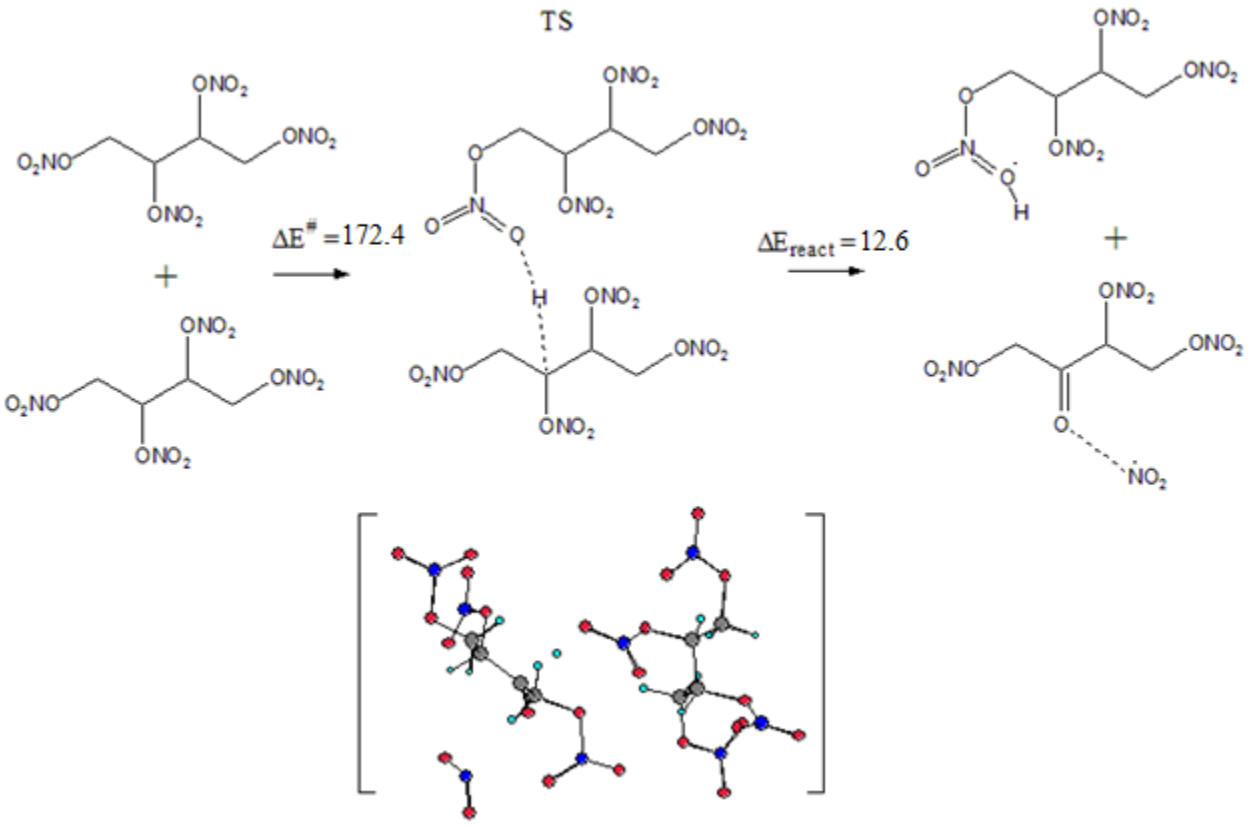

Figure 7: ETN starting reaction (H-atom transfer between two ETN molecules) in intermolecular decomposition routes. Energy values are given in kJ/mol.

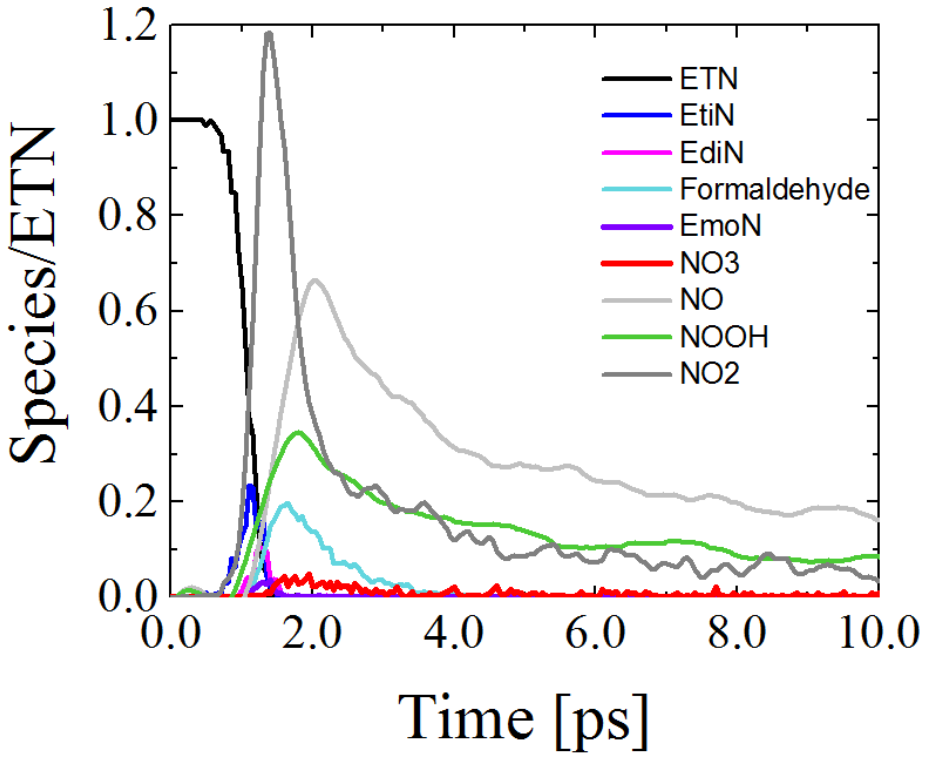

Figure 8: Calculated initial decomposition species of bulk ETN. The first 10ps are shown with the major intermediate species. Values are normalized to initial amount of ETN molecules.

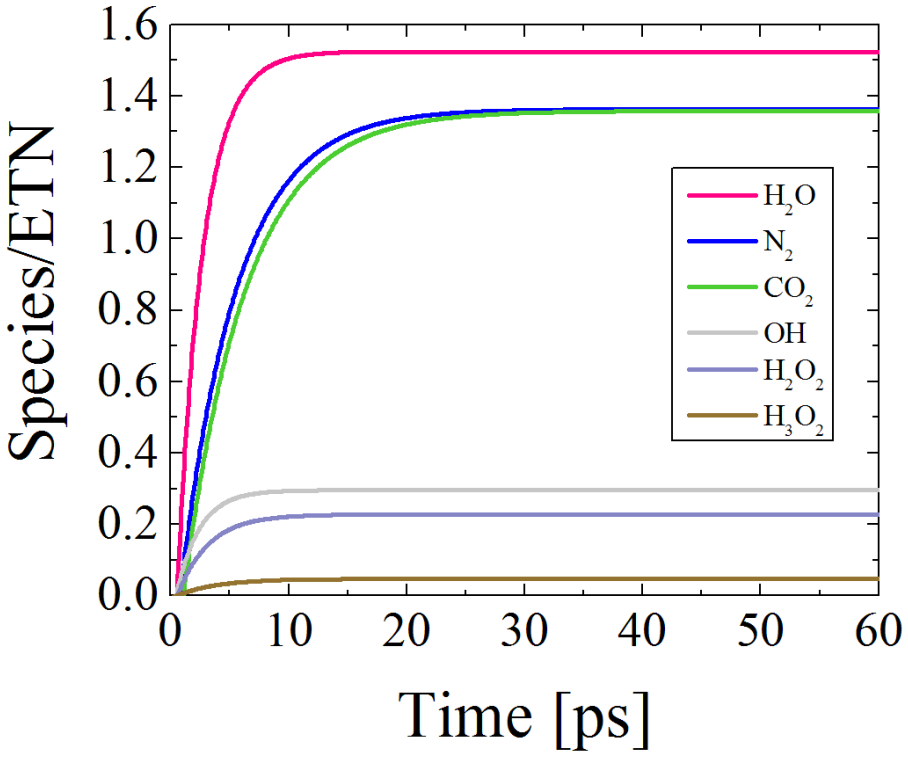

Figure 9: Calculated thermodynamically stable decomposition products obtained in decomposition of bulk ETN at simulated detonation conditions, P_{CJ}=26GPa and T_{CJ}=4300K. Values are normalized to initial amount of ETN molecules.

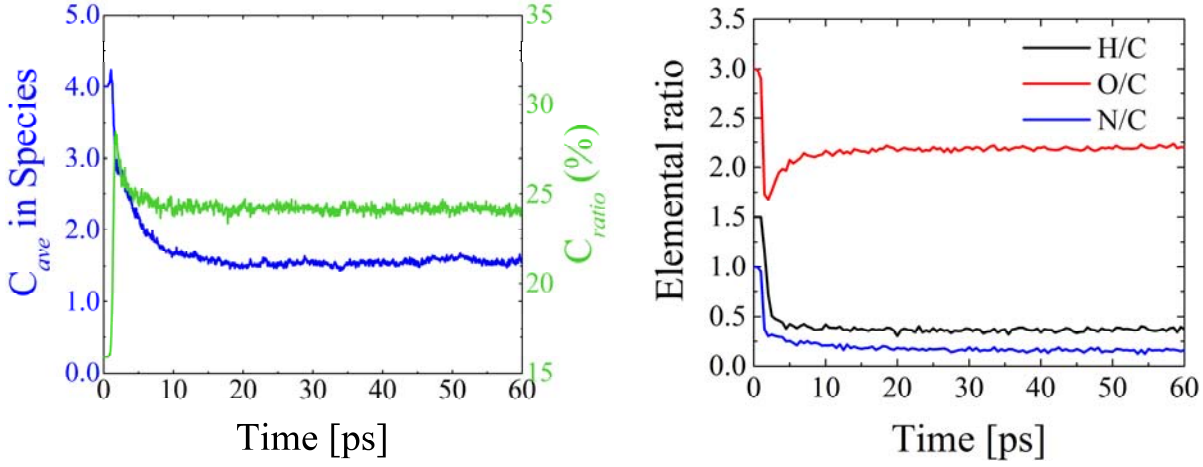

Figure 10: Left panel: Calculated average number of carbon atoms in a molecule colored in blue, and percent of carbon atoms in green. Right panel: Calculated elemental ratios in carbonaceous species during decomposition.

a)

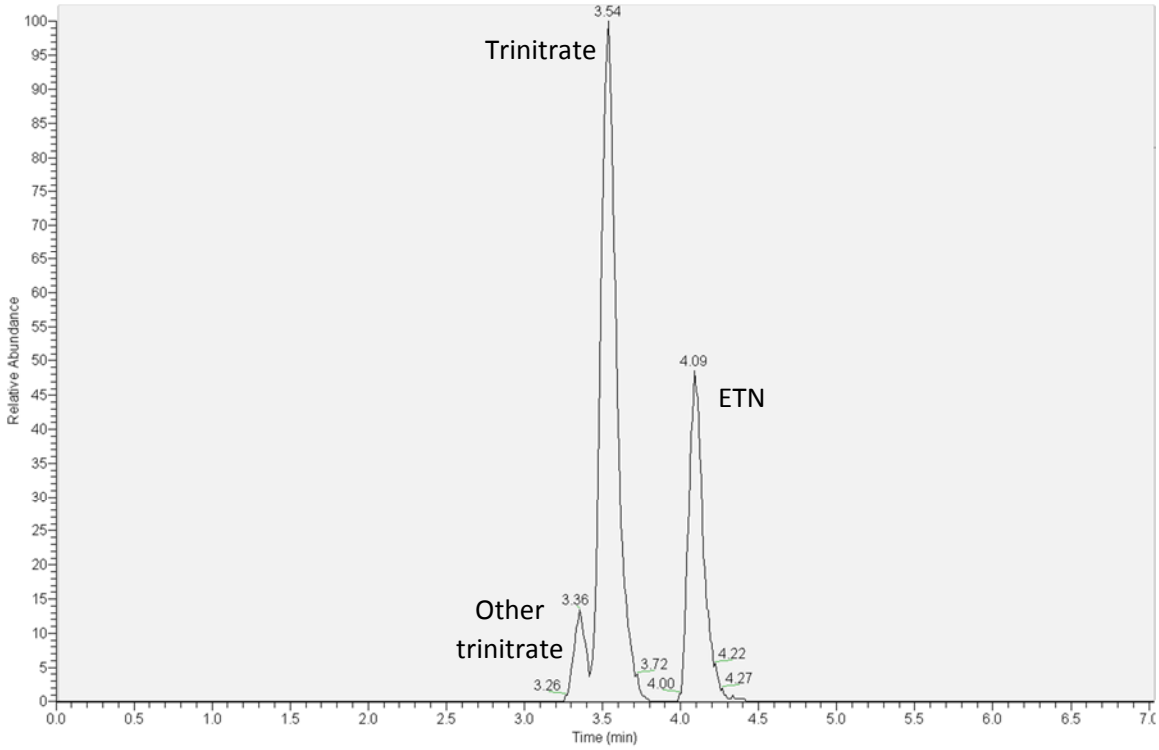

b)

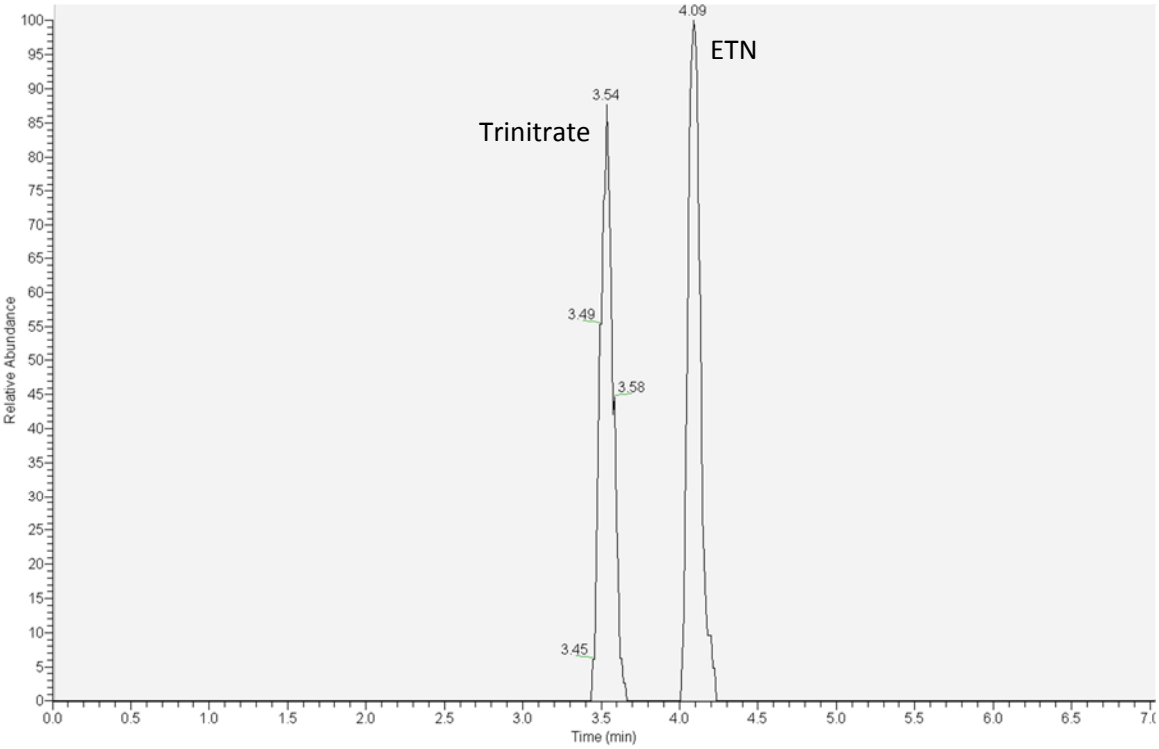

Figure 11: Extracted ion chromatograms (291.9825) of partially a) nitrated b) decomposed

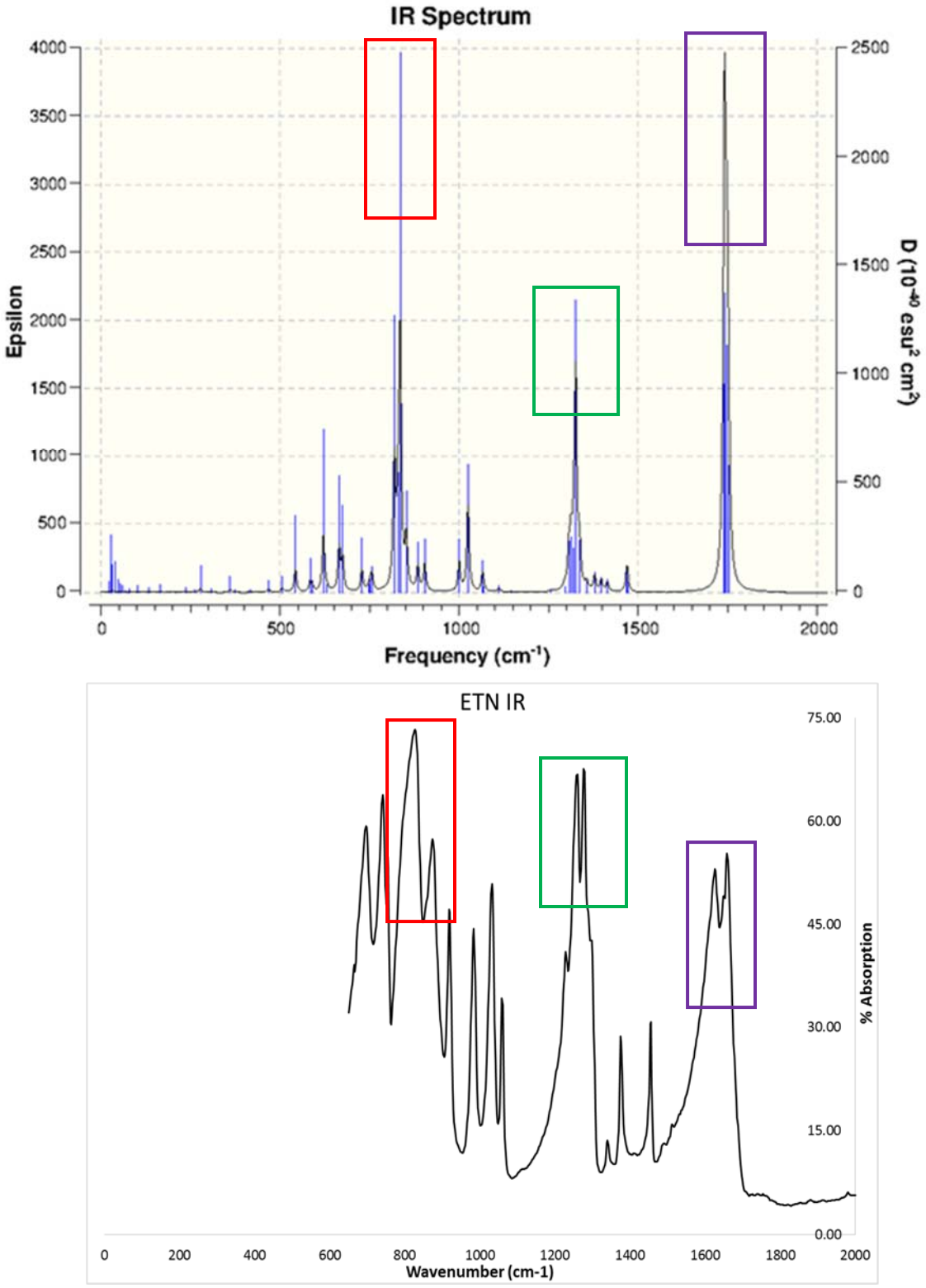

Figure 12: IR of ETN, DFT (top), Experimental (bottom). Red: ONO Scissoring (Calc: 820-854 cm^{-1}, Exp: 827-874 cm^{-1}); Green: Symmetric NO_2 stretching (Calc: 1326-1337 cm^{-1}, Exp: 1259-1277 cm^{-1}); Purple: Asymmetric NO_2 stretching (Calc: 1741-1753 cm^{-1}, Exp: 1626-1659 cm^{-1})

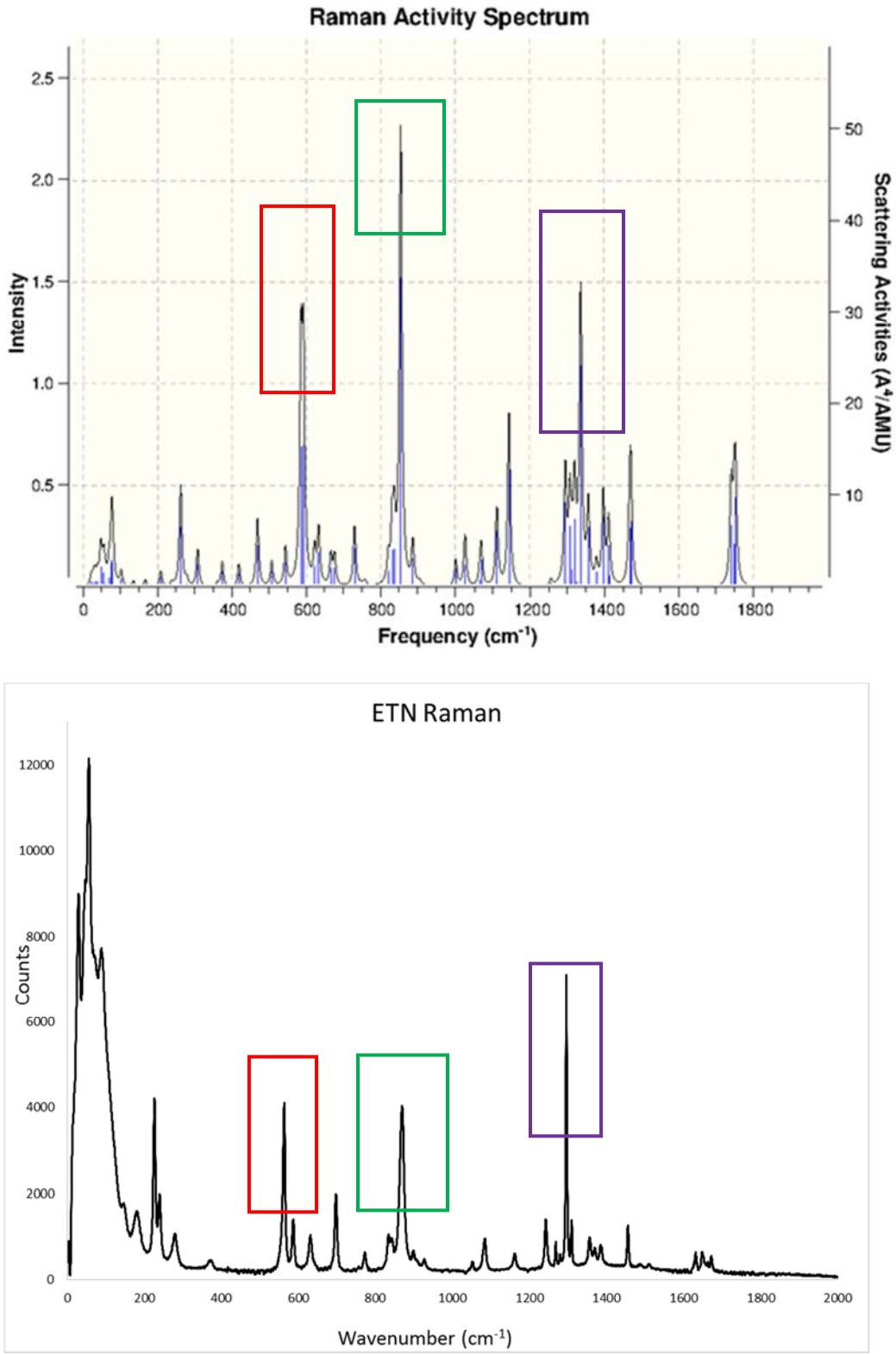

Figure 13: Raman of ETN, DFT (top), Experimental (bottom). Red: OCH rocking (Calc: 586-592 cm^{-1}, Exp: 564 cm^{-1}); Green: NO2 Scissoring (Calc: 854 cm^{-1}, Exp: 870 cm^{-1}); Purple: NO2 symmetric stretching (Calc: 1337 cm^{-1}, Exp: 1296 cm^{-1})

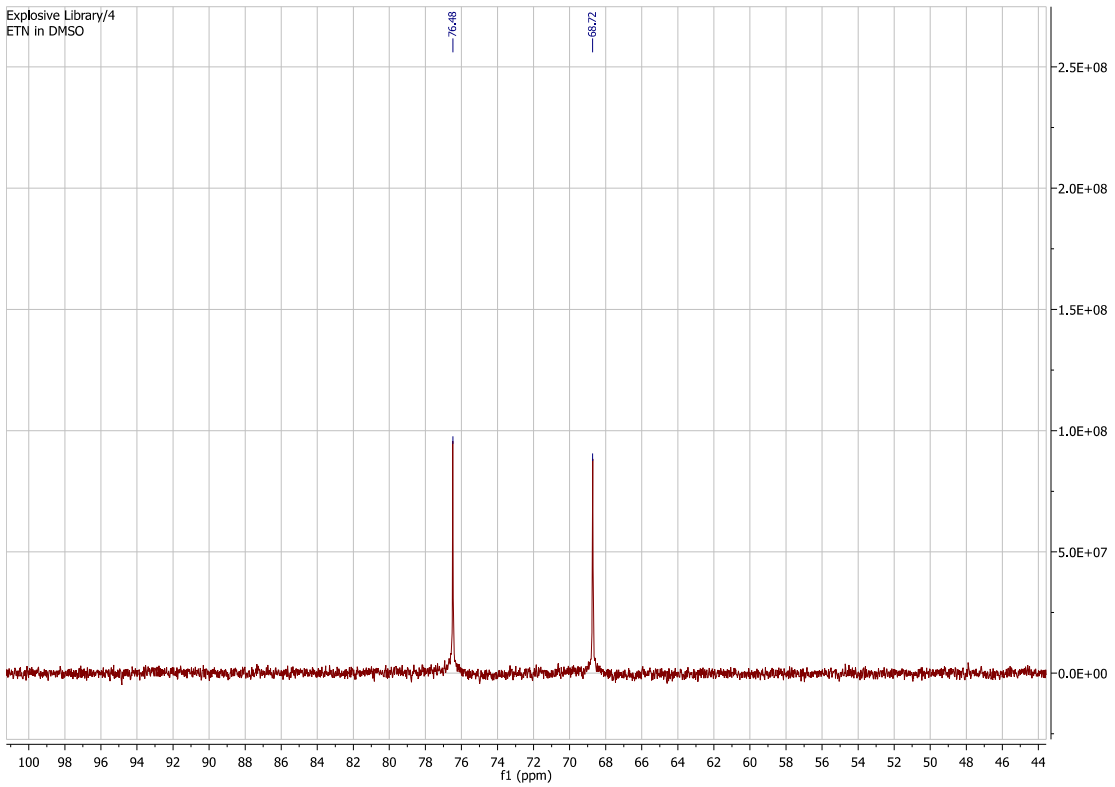

Figure 14: Carbon NMR of ETN.

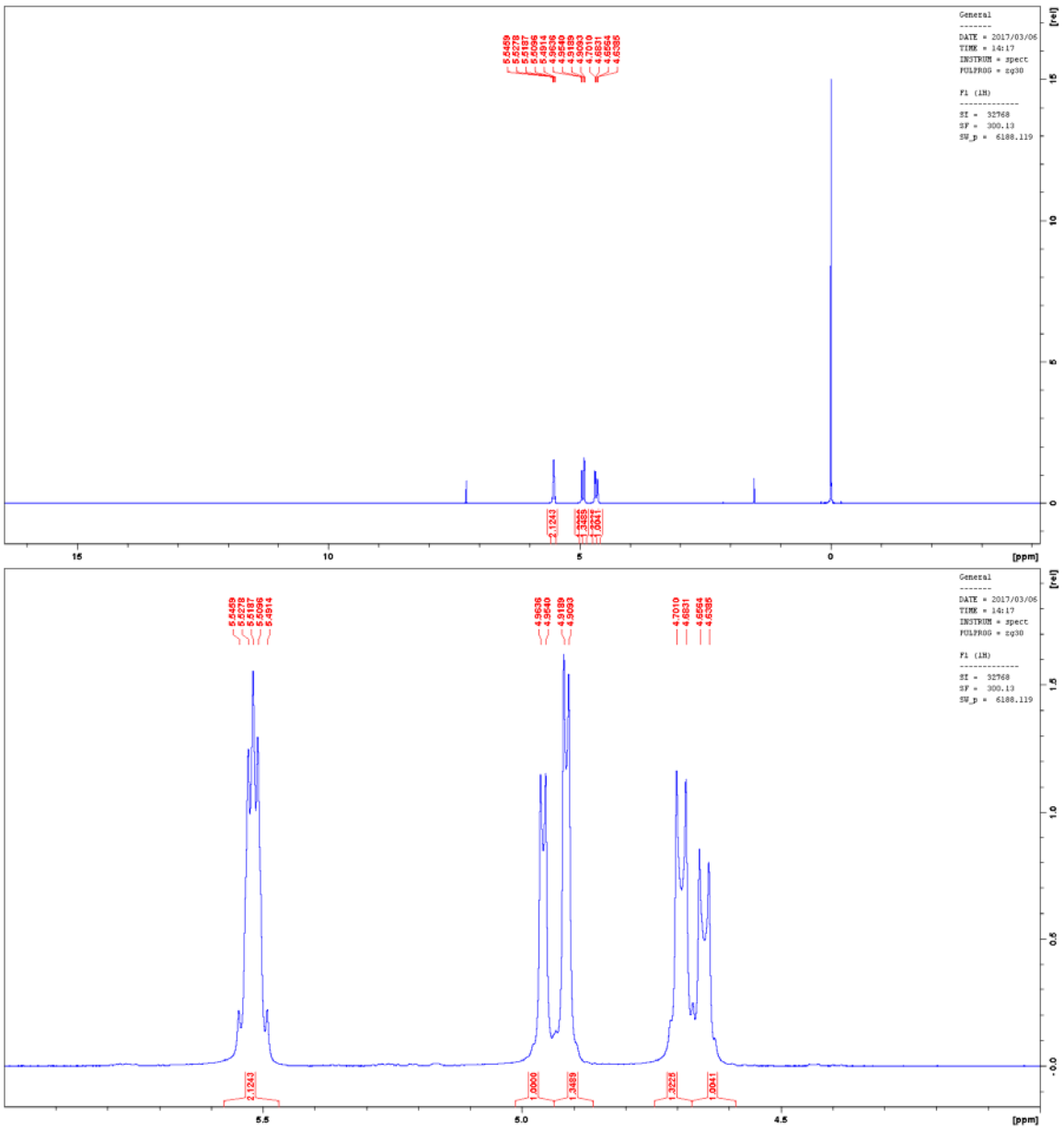

Figure 15: Proton NMR of ETN in $CDCl_3$